Published in final edited form as:
Nat Astron. 2019 ; 3: 543–552. doi:10.1038/s41550-019-0726-y.

Evolution of Saturn's Mid-Sized Moons

Marc Neveu[1,2] **Alyssa R. Rhoden**[3]

[1]Department of Astronomy, University of Maryland, College Park, MD, USA.

[2]CRESST II and Planetary Environments Laboratory, NASA Goddard Space Flight Center, Greenbelt, MD, USA.

[3]Southwest Research Institute, Boulder, CO, USA.

Abstract

The orbits of Saturn's inner mid-sized moons (Mimas, Enceladus, Tethys, Dione, and Rhea) have been notably difficult to reconcile with their geology. Here, we present numerical simulations coupling thermal, geophysical, and simplified orbital evolution for 4.5 billion years that reproduce observed characteristics of their orbits and interiors, provided that the outer four moons are old. Tidal dissipation within Saturn expands the moons' orbits over time. Dissipation within the moons decreases their eccentricities, which are episodically increased by moon-moon interactions, causing past or present oceans in the interior of Enceladus, Dione, and Tethys. In contrast, Mimas' proximity to Saturn's rings generates interactions that cause such rapid orbital expansion that Mimas must have formed only 0.1–1 Gyr ago if it postdates the rings. The resulting lack of radionuclides keeps it geologically inactive. These simulations can explain the Mimas-Enceladus dichotomy, reconcile the moons' orbital properties and geological diversity, and self-consistently produce a recent ocean on Enceladus.

The moons' ages are debated. Their crater distributions, assuming Sun-orbiting impactors extrapolated from present-day observed small body populations, suggest surfaces billions of years old[1]. Conversely, the measured fast expansion of their orbits[2], likely due to tides raised by the moons on Saturn, indicates – assuming dissipation levels constant over time and frequency of tidal excitation – that this relatively compact moon system is less than a billion years old. This could explain why some moons may not have encountered predicted orbital resonances[3], and supports scenarios of non-primordial formation from debris of the tidal or collisional disruption of progenitor moons[4–6].

The moons' widely different bulk densities (i.e. rock contents or bulk porosities) and internal structures are surprisingly uncorrelated with mass or distance to Saturn (Table 1). Formation

---

Materials and correspondence: Requests for materials and correspondence should be addressed to M. Neveu (marc.f.neveu@nasa.gov).

Author contributions

M.N. developed the models and ran the simulations. M.N. and A.R.R. designed the research and interpreted the results.

Competing financial interests

The authors declare no competing financial interests.

from a debris ring could first result in stochastic accretion of rock seeds more resistant than ice to tidal disruption, then coated by ice shells as the moons raise tides on Saturn, move outward, and experience lower tidal stresses[7]. Enceladus and Dione have low-density ($\approx$2400 kg m^{-3}) rocky cores and ice shells[8–10], Mimas too is differentiated[11], whereas Rhea, the largest moon and thus most prone to retaining endogenic heat, seems homogeneous[12]. Tethys' interior is unconstrained.

The contrast in tidally driven geological activity between Mimas and Enceladus is also exceptional. Enceladus harbors a global ocean[13] interacting with the rocky core[14;15] and venting to space[16] in an area of high heat flow[17–19]. On Mimas' closer-in, more eccentric orbit, saturnian tides should be 30 times stronger[20]. Yet, Mimas shows no geological activity[1;21]. This dichotomy must arise from their differing propensity to deform due to tides, as previously postulated[22–24] but not elucidated.

In order to model the effect of tidal coupling on the properties of the moons, both geophysical (billion years) and orbital (daily) timescales need to be considered, which is currently unachievable. For this reason, previous approaches have prescribed either orbital[25;26] or interior properties[3;7;27].

Here, we present simulations of the moons' orbits, degree of differentiation, and internal activity over time. The coupled thermal, geophysical, and orbital evolution of all five moons is concurrently simulated from formation to the present day. Our 1D simulations (see Methods) compute rock-ice differentiation, heat transfer, parameterized convection in the core, ocean, and shell, and porosity compaction. Semi-major axes and eccentricities change due to tidal dissipation in Saturn and in the moons, moon-ring interactions, and mutual gravitational interactions between moons approximated as repeated conjunctions to address the timescale issues[7]. We validate this approach against an averaged-Hamiltonian model of resonant interactions between moon pairs[28]. We assume that some moons form from Saturn's rings[7], and thus that the rings predate at least these moons. Measurements of the rings' masses, silicate contents, and infall micrometeoroid fluxes suggest the rings are young[29;30], contradicting this assumption, but proposed origin scenarios favor either much older rings[5;31;32] or a common origin for the rings and the moon (Mimas) that accretes from them[33].

Saturn's tidal quality factor Q (inverse of the mean angle between the actual and frictionless tidal bulges) is arbitrarily decreased linearly over time to 2452.8, the geometric midpoint of the present-day range[2]. A constant Q in this range leads to non-primordial inner moons. Assuming higher past values allows us to probe scenarios with older moons. We neglect any dependence on excitation frequency, as Q seems currently uniform within an order of magnitude at the moons' orbital frequencies[2] and cannot yet be quantitatively predicted from evolutionary models of Saturn's interior. Qualitatively, a linearly decreasing Q may emulate an effective decrease linked to the evolution of Saturn's internal structure, if dissipation inside Saturn takes place by fluid waves with velocities commensurable to the moons' orbital velocities[34].

The moons start closer to Saturn than today, because angular momentum transferred from Saturn's relatively faster spin into their orbits tends to increase orbital semi-major axes a more than tidal dissipation inside the moons decreases them (equation 4 in Methods). Plausible starting positions are computed by integrating the second term of equation (4) backward in time to produce the $a(t)$ curves shown in Fig. 1. Moons beyond the outer ring radius R_{out} at $t = 0$ are assumed primordial. Otherwise, they are spawned from the rings when their orbit is slightly beyond R_{out}.

Initial conditions (Tables 1 and 2), model upgrades, and simplifying assumptions are further discussed in Methods and Supplementary Material.

A young Mimas and an old Rhea

To constrain some parameters of the initial satellite system, we determine age limits on Mimas and Rhea from examination of their tidal relationships with the rings and Saturn, respectively. Moon-ring interactions hasten orbital expansion out to $a = 222000$ km, where the lowest-order inner Lindblad resonance leaves the rings' outer edge[7]. Today, these interactions affect only Mimas' orbit (Table 1), expanded from $a = 160000$ km in ≈ 1.1 (10^{19} kg/M_{ring}) billion years (Gyr), i.e. ≈ 0.14 to 1 Gyr for $M_{ring} = 1.1 - 8 \times 10^{19}$ kg[35;36]. Preliminary *Cassini* gravity measurements suggest $M_{ring} \approx 1.8 \times 10^{19}$ kg[36], within this range. Expansion from $a = 140000$ km, the current outer edge of the dense rings, to 160000 km is even faster because of additional higher-order Lindblad resonances (equation 2). Thus, Mimas must be younger than ≈1 Gyr if predated by Saturn's rings[5], otherwise Mimas-ring interactions would have widened its orbit beyond today's. Alternatively, a primordial Mimas would require younger rings and a poorly dissipative Saturn.

Conversely, Rhea is likely primordial, even for a low Saturn Q. Although we neglect this dependence in our simulations, Q varies with time and orbital frequency (semi-major axis). Since today $Q(a, t) = 1500–5000$ for Enceladus, Tethys, and Dione and 300 for Rhea[2], we assume for this argument that $Q(a) > 1650$ out to 500000 km (between Dione and Rhea) and 300 beyond. Provided this frequency-dependent Q was constant through time, it took > 4.6 Gyr for Rhea's orbit to expand from the rings' outer radius by tides raised on Saturn. Rhea-ring interactions hasten early expansion, but dissipation inside Rhea moderates it. For higher, likelier past values of Q, Rhea is primordial. Early migration is even slower if Rhea progressively accreted from less massive moons[7] raising weaker tides, but previous work has shown that for a low Saturn Q, a Rhea-sized moon forming from the rings accretes most of its mass within just a few million years (Myr)[7].

Consequently, in our explored scenarios, Mimas is spawned from the rings at a time that depends on M_{ring}, Rhea is primordial, and the other moons fall into either category depending on Saturn's initial Q. Primordial moons are assumed to accrete homogeneous and differentiate if heated enough. Moons spawned from rings are assumed to form layered into a rocky core and ice shell on the grounds that a more cohesive rock-rich seed accretes first[7]. In either case the core, assumed to retain ≈25% water-filled porosity[37;38] has density $\rho_c = X_{ice}\rho_i + (1 - X_{ice})\rho_r = 2421$ kg m^{-3} (Table 2), consistent with constraints for Enceladus and

Dione (Table 1). The core water volume fraction is too low to dominate the rheology of the (assumed well-mixed) rock-ice mixture, as ice grains are on average not adjoined.

The canonical case

We first assume an initial Saturn $Q = 80000$, the lowest value for which all moons except Mimas are primordial. We set $M_{ring} = 1 \times 10^{19}$ kg, 4.5–8 times lower than estimated[35] to reflect the lower surface density of the A ring with which moons solely interact for $a \geq$ 190000 km. Setting $M_{ring} = 5 \times 10^{19}$ kg yields similar results (Supplementary Fig. 1). A starting eccentricity $e = 0.016$ is assumed for all moons (see Methods). The resulting orbital a and e; internal temperatures; and core, ocean, and shell radii are respectively shown in Fig. 2a, c, and d. The four outer moons start with eccentricities higher than today. At initial uniform temperatures set to 100 K, their interior ice is poorly dissipative. Therefore, early heating is predominantly radiogenic and depends on each moon's rock content, especially since hydrated rock is more insulating than cold crystalline ice. As the moons warm up in the first 500 Myr (Fig. 2c), increased dissipation in compacted, less viscous ice circularizes their orbits (Fig. 2a). Dione and Rhea differentiate (Fig. 2d). Rhea sustains a ~100-km thick ocean for the next 1.5 Gyr until it refreezes as radiogenic heating decreases. Tidal heating remains comparatively negligible owing to Rhea's low eccentricity. Dione has no ocean (liquid water outside its core), but harbors pore liquid water in the core (Fig. 2d).

About 2.8 Gyr after formation, Tethys and Dione enter a 3:2 mean-motion resonance that excites their orbital eccentricities, generating enough dissipation that their orbits contract. Enceladus' expanding orbit and Tethys' contracting orbit converge into a 4:3 mean-motion resonance (Fig. 2b), raising Enceladus' eccentricity (but not that of Tethys, which is already high; equation 6 in Methods). Our simplistic model computes a sudden increase from $e \sim 10^{-7}$ to 0.5 (Fig. 2a). Using a more sophisticated treatment of moon-moon interactions similarly leads to fast excitation to $e > 0.1$ (Supplementary Sections 2 and 3), suggesting that this behavior is robust. The resulting tidal dissipation, equivalent to that produced for an eccentricity ≈ 0.1 (see Methods), results in runaway heating. As the ice viscosity decreases, Enceladus becomes more dissipative and gets warmed further. Ice melts in the innermost zones, triggering global differentiation. Meltwater circulates throughout the porous core, distributing the tidal heat from the shell throughout the interior to a homogeneous 300–400 K (Fig. 2c). Core porosity arises from the thermal pressurization of pore water (see Methods) assumed trapped in rock during differentiation. Some porosity could also remain from the sedimentation of rock grains. Thus, Enceladus develops an ocean (Fig. 2d) that persists for 1 Gyr but refreezes as Enceladus' eccentricity decreases quickly from 0.07 at 3.9 Gyr to 0.0007 at 4.0 Gyr. Freezing could be stalled by resonant ocean tidal heating[39], neglected in our model. Enceladus then returns to its pre-3 Gyr state of quiescence. Its eccentricity stabilizes to a few 10^{-4}, then increases slightly due to dissipation inside Saturn.

The 3:2 Tethys:Dione resonance leads to Tethys maintaining an ocean from 3.1 Gyr to the present. Dione's ice shell also melts briefly then, and again at 3.7 Gyr when in 7:4 resonance with Rhea (whose eccentricity is already high enough to avoid excitation).

At 3.4 Gyr, Mimas is spawned from the rings and, gravitationally interacting with them, quickly recedes to its current orbit. Its eccentricity is too low for its poorly dissipative interior to experience much tidal heating, and too high to be affected by moon-moon resonances.

Simulation outcomes bear striking commonalities with the present-day Saturn system (Table 3). Radii and bulk densities are matched within 5%. Computed core sizes are within the ranges reported in Table 1. A simulation snapshot taken between 3 and 4 Gyr reproduces an ocean on Enceladus, hydrothermally circulating through its rocky core, with temperatures of 300–400 K that match those (≥ 323–363 K) inferred from analyses of plume material[14;40]. Computed mean global heat fluxes across Enceladus' ice shell, 25–100 mW m^{-2} (20–80 GW total heat output rate), are bracketed by present-day measurements of 4.2–15.8 GW just around the tiger stripes[18;19] and past fluxes estimated from relaxation of surface features (Table 1). A possible ocean on Dione[8] is also reproduced, with corresponding computed heat flows of 70–85 mW m^{-2} through its upper ice shell comparable to reported estimates (Table 1). So are Rhea's, computed to reach 12 mW m^{-2} at 2.4 Gyr. The simulation results in a compositionally layered yet geologically inactive Mimas, as observed[11]. Despite approximated disk torques and N-body interactions, the model reasonably reproduces the present-day orbits of all mid-sized moons. At 4 Gyr, the semi-major axes of Mimas and Rhea are within 0.5% of today's, although Enceladus, Tethys, and Dione are slightly too close in by 12, 20, and 7%, respectively. Therefore, Enceladus and Dione are not in a 2:1 mean-motion resonance. The match is better at 4.5 Gyr: within 3, 9, and 5%, respectively, due to our choice of initial semi-major axes (Table 1). The range of eccentricities experienced by each moon includes its present-day value. Mimas' eccentricity, whose computation ends up depending only on interactions with Saturn, matches its observed value within a few percent.

Varying initial conditions

Some outcomes change when varying initial values for Saturn's Q and initial orbits accordingly (Supplementary Table 1). If initially $Q = 200000$ (simulation not shown), neither Enceladus nor Dione have oceans: both undergo only a weaker resonance with Mimas (5:3 at 3.4 Gyr and 3:1 at 3.9 Gyr, respectively), which does not raise their eccentricity enough to trigger melting, owing to Mimas' relatively low mass. Dione excites Tethys' eccentricity at 3.8 Gyr, but Tethys' interior is too cold then for even high-eccentricity dissipation to cause melting or differentiation.

An initial $Q = 50000$ requires that both Mimas and Enceladus form past 3 Gyr, layered, from the rings (Supplementary Fig. 2). Enceladus never has an ocean: although its eccentricity is significant, its cold interior, in part due to the lack of live radionuclides accreted, is not sufficiently dissipative to elicit positive tidal feedbacks. In the first 2 Gyr, Tethys, locked in a 2:1 resonance with Dione, undergoes repeated eccentricity excitation roughly every 400 Myr, causing a repeating pattern of increased temperatures and melt (Supplementary Fig. 2e,f). High dissipation in both moons maintains their orbits at relatively constant semi-major axes. Furthermore, Tethys' semi-major axis is kept at a minimum of 222000 km owing to its interactions with rings about four times as massive as today, which incorporates the material

that later spawns Enceladus, then Mimas. The system's evolution is otherwise similar to the above cases and to the $Q = 20000$ scenario (Supplementary Fig. 3), in which Tethys too forms late at ≈ 3 Gyr.

With $Q = 2452.8$ constant over time (Fig. 3), all moons except Rhea form late. Orbits expand promptly, especially when close to the rings. For this simulation, the final ring mass is arbitrarily higher (7×10^{19} kg, within the estimated range[35]); a lower mass would make the late-forming moons older. As in the other $Q \leq 50000$ cases, Mimas and Enceladus never have an ocean, but Rhea, Dione, and even a young Tethys do.

Simulations (not shown) with starting eccentricities 10 and 100 times lower than 0.016 for primordial moons and $Q = 10^5$ produce less dynamical and geological activity in the system. Enceladus' eccentricity is only excited once (5:3 resonance with Mimas), and not sufficiently to provoke melting and differentiation. This could be due to a fortuitous lack of mean-motion resonances, compounded with less opportunities for crossing mean-motion resonances because of slow early migration at high Saturn Q and less orbital contraction in the absence of strong tidal dissipation in the moons.

Thus, varying starting Q, orbital positions, and eccentricities results in simulations not matching quite as well observational constraints (Table 3), even though salient features are retained: Mimas forms late and remains cold, Rhea is primordial and radiogenically heated, and the other moons can undergo moon-moon interactions that raise their eccentricities, triggering episodes of high tidal dissipation so long as the moons' interiors are sufficiently warm and therefore dissipative.

Discussion

Matching the present-day Saturn system requires a high initial Saturn Q such that Enceladus, Tethys, Dione, and Rhea form early on. Late-forming moons seem less prone to have interacted with other moons because their initial outward migration is dominated by interactions with the ring[7]. This ring-dominated regime seems a robust result, but should be confirmed with more faithful models of moon-moon interactions. In late-forming moons, radiogenic heating is negligible, further preventing the onset of significant dissipation in frigid interiors.

This provides an interpretation for the Mimas-Enceladus dichotomy: Mimas formed less than 1 Gyr ago from Saturn's rings; whereas Enceladus formed earlier (possibly in the Saturn subnebula), underwent dynamical excitation by interacting with other moons (primarily Tethys and Dione), consequently experienced high levels of tidal dissipation, and its orbit is currently circularizing such that it is out of tidal equilibrium[41;42]. This explanation for Enceladus' extraordinary internal activity has been proposed[25;26], but not modeled consistently with the long-term evolution of the whole inner Saturn system. Observations are best matched at ≈4 Gyr into the simulation, close to today's 4.57 Gyr. Mimas' time of formation from the rings hinges on their mass, but is too late for radiogenic or even tidal heating to be significant. This could yield a possibly unrelaxed core[11;20], although our computed lack of pore compaction in the shell is at odds with Mimas'

relatively relaxed shape[43]. Since Mimas is heavily cratered, a formation less than 1 Gyr ago would strongly constrain impact source populations, including secondaries, sesquinaries, and planetocentric debris[1].

Our results suggest that Saturn's rings predate at least Mimas (or that the rings are young, but Mimas is not), but because the evolution of the other moons (if primordial) is insensitive to the presence or mass of the rings, these moons do not further constrain their origin. Thus, both primordial or more recent rings remain viable scenarios[5;31]. In particular, the canonical scenario is fully compatible with an origin for Mimas and the rings < 1 Gyr ago from the disruption of a common parent moon[33]. More generally, it implies rings orders of magnitude less massive than rings resulting from the tidal disruption of a Titan companion[5], but compatible with the collisional disruption of a primordial small moon[31]. In this scenario, Enceladus' early orbital expansion is also sped up by interactions with the rings, but equivalently Enceladus could have formed before the rings and about 220000 km from Saturn (Fig. 2a, extrapolating $a(t)$ between 0.5 and 2.8 Gyr back in time to 0 Gyr). This may justify our prescribed and otherwise puzzling lack of moon formation by ring viscous spreading in the long interval between the formations of Enceladus and Mimas.

Our simulations, including the canonical case, result in eccentricities above 0.1. These would result in orbit crossing and, perhaps, collisions[3;4]. Reaccreted moons would likely have lost any stored radiogenic heat, which could be compensated by accretional heating. Their orbits would likely differ from their progenitors'.

Results that consider resonance capture (Supplementary Fig. 9) suggest that Enceladus and Dione could remain at or near the 2:1 resonance for several Gyr, as was previously found assuming a constant Q for Saturn and the moons[28]. With slightly different initial orbits, the resonance can be exited after 20 Myr due to eccentricity pumping of both moons (Supplementary Fig. 8) or capture avoided altogether (Supplementary Fig. 7) because Dione's eccentricity is excited by prior passage through a 3:2 resonance with Tethys. In our simulations, this 3:2 resonance is much more easily broken (after 14 Myr, Supplementary Fig. 7–9) than in a previous study[27] for k_2/Q values similar within an order of magnitude, maybe because k_2/Q is varied with tidal dissipation in our model. This resonance could also be broken due to inclination excitation[3], which we did not model.

The lack of resonance capture in the repeated encounter model could considerably affect the simulated moon dynamics and thermal states. Resonances induce relative changes in semi-major axes $\Delta a/a \propto e^2$ (ref.[44]), i.e. ~1% for excitation of $e \ll 1$ to $e \approx 0.1$. This translates to differences in tidal dissipation (proportional to $a^{-7.5}$) of about 10%. More importantly, because of slow secular expansion, the timing of subsequent orbital resonances is sensitive to the relative a of the moons, differing by > 1 Gyr if the a of one moon is changed by only < 1.5% (cf. Enceladus and Dione in Supplementary Table 1 and Fig. 7–9). Moreover, the duration of orbital resonances and corresponding tidal dissipation forcing depend sensitively on pre-resonance conditions[44]. With only slight variations of the age and initial positions of Enceladus and Dione, their 2:1 resonance can last Gyr, Myr, or not occur at all (Supplementary Section 2). The repeated encounter model best approximates brief (Myr) resonance durations that punctually excite eccentricities, but fully accounting for resonance

capture (e.g. with N-body simulations) could result in much more prolonged or much less heating. The results of this work must be interpreted with these caveats in mind: our simplified model can reproduce much of the inner Saturn system, but other families of solutions also compatible with observations may be identified as the space of initial conditions is more systematically explored with higher-fidelity models of orbital evolution.

We have assumed that moons spawned from rings were fully formed upon reaching a = 160000 km. More continuous accretion[7] from less massive proto-moons that raise weaker tides on Saturn would imply slower orbital expansion, and further lessen the role of radioactive heating – dissipated faster in smaller bodies–, but imply a role for impacts in affecting both interiors and orbits.

Beyond reproducing the best available constraints on the moons' internal structures, our models suggest that a primordial Tethys must have differentiated, and likely experienced past episodes of high heat flow (up to 50 mW m^{-2}) consistent with surface evidence (Table 1). The cores of Enceladus, Dione, and Rhea are much larger than expected from the full differentiation between silicates and ice. Such low-density cores, consistent with observations, can be maintained over geologic time if the rock maintains ≈25% water-filled porosity[37;38]. Deep pore water in the core, better insulated from the surface, is melted more easily than in the shell, promoting water-rock interaction in the moons' interiors.

Methods

Interior-orbital evolution code

We model the thermal evolution of each icy moon using a routine created by Desch et al.[54], which performs time-dependent calculations of the internal temperature profile and structure of bodies made of rock and ice, including the effects of differentiation[55]. This code was modified to include a detailed model of the effects of core fracturing, hydrothermal circulation, rock hydration and dehydration[56], as well as tidal heating (as a function of depth, temperature, and composition) and porosity[20]. Self-compression is neglected.

Mass is distributed assuming spherical symmetry on a fixed-volume one-dimensional grid, with a specified number of zones (here, 200) evenly distributed in radius. The internal energy in each grid zone is computed from the initial temperature using equations of state for rock and ice (here assumed to be pure water). Accretional heating is assumed dissipated before the simulation starts. Rock and radionuclides are assumed to be solely in the core (no mud in oceans or ice shells and no leaching of ^{40}K). A thermal structure is determined by balancing conductive heat transfer with radiogenic (long-lived radionuclides only; abundances from Lodders[57]), gravitational[54], chemical[56], and tidal heating[20], using a finite-difference method and a 50-year time step. Thermal conductivities depend on composition, temperature, and porosity[20]. Tidal dissipation due to orbital eccentricity is computed by solving the equations of Tobie et al.[58] with a propagator matrix technique[42;59] assuming an Andrade model for the response of non-Newtonian rock, ice, and rock-ice mixtures to tidal forcing[20]. Fluid tides are ignored, even though they could induce major heating in moons with an ocean[39]. Porosity can compact at rates set by material viscosities. Volume changes due to ice melting or freezing are neglected. Enhanced heat transfer is computed in the ice

shell and/or fractured core (hydrothermal circulation) if the Rayleigh number appropriate for convection between two plates or for porous media, respectively, exceeds a critical value[56]. In such grid zones, an effective thermal conductivity is computed through multiplication by the Nusselt number (ratio of convective to conductive heat fluxes, a function of the Rayleigh number[54]). In liquid grid zones, an effective thermal conductivity is set to 400 W m^{-1} K^{-1}, high enough to yield a nearly isothermal liquid layer, yet sufficiently low to satisfy the Courant criterion.

The evolution of a moon's orbit is computed only in terms of its semi-major axis a and eccentricity e; spin and orbital planes are assumed coplanar with Saturn's equator and rings. The lack of consideration of orbital inclinations prevents us from using these as an additional, useful constraint on the history of the system[3]. In our previous models[20], a moon's orbit changed solely due to tidal dissipation inside this moon (which decreases a and e) and inside Saturn (which increases them, since Saturn spins faster than the moons orbit). For the present study, we have added the effects of moon-ring and moon-moon interactions as follows.

Moon-ring interactions

We model moon-ring interactions arising from Lindblad resonances[7]. These occur when ring particles and a moon exterior to the rings have mean motions in the ratio k:(k − 1), where k is a positive integer[60]. Lindblad resonances also occur for moons interior to rings, but are not relevant here. Such interactions result in a torque Γ between the moon and the rings, of magnitude (equation 16 of Meyer-Vernet & Sicardy[60]):

$$\Gamma = \sum_k \Gamma_k = \sum_k \frac{4}{3}\pi^2 \frac{\Sigma A_k^2}{\Omega_k \omega} \quad (1)$$

where Γ_k are individual torques arising from Lindblad resonances of order k; $\omega = \sqrt{GM/a^3}$ is the orbital frequency of the moon, with G the gravitational constant and M the mass of Saturn; $\Omega_k = \omega k/(k-1)$ is the orbital frequency of ring particles; and Σ is the ring surface density, which we approximate as $\Sigma = M_{\text{ring}}/\left[\pi\left(R_{\text{out}}^2 - R_{\text{in}}^2\right)\right]$ with M_{ring}, R_{out}, and R_{in} the ring mass, outer radius, and inner radius, respectively. A_k is the product of $Gm/2a$, with m the moon's mass, and a term of order k (equations 9 and 17 of Meyer-Vernet & Sicardy[60]); we approximate it as $A_k \sim GMk/2a$. Thus:

$$\Gamma \sim \sum_k \frac{1}{3}\pi \frac{M_{\text{ring}}\, G\, m^2 a\, k(k-1)}{\left(R_{\text{out}}^2 - R_{\text{in}}^2\right)M} \quad (2)$$

The ring exerts a torque Γ on the moon, whereas the moon exerts a torque −Γ on the rings; i.e., the moon and the rings repel each other[60]. In practice, the calculation of Γ involves summation over only a few k terms, unless the moon is very close to the outer edge of the

rings: $a < \left[R_{\text{out}}^{3/2}\, k/(k-1)\right]^{2/3}$, which corresponds to 150000 km for $k = 10$, assuming R_{out} = 140000 km. Beyond 222000 km, the lowest-order ($k = 2$) resonance leaves the rings and ring torques no longer affect the moon's orbital evolution[7]. Because Saturn's A and B rings are the densest and most massive, we neglect the C and D rings and assume a constant surface density between R_{in} = 92000 km (inner edge of the B ring) and R_{out} = 140000 km (radius of the narrow F ring, just outside the A ring).

This torque is assumed to only affect orbital semi-major axes, although it has been argued that eccentricities may be affected too[61]. Its effect on orbital expansion is[7]:

$$\frac{da}{dt} = \frac{2a^{1/2}\Gamma}{m(GM)^{1/2}} \quad (3)$$

We add this term to equation (14) of Neveu & Rhoden[20] to compute the net change in a moon's semi-major axis due to tidal dissipation inside this moon (first term below), tidal dissipation inside Saturn (second term), and moon-ring interactions (third term):

$$\Delta a = \Delta t \times \left(\frac{-2\sum_i Q_{i,\,\text{tide}} a^2}{GMm} + 3\frac{k_2}{Q}\frac{\sqrt{GM}R_p^5 m}{a^{5.5}} + \sum_k \frac{2}{3}\pi \frac{M_{\text{ring}}\, G^{1/2} m\, a^{3/2} k(k-1)}{\left(R_{\text{out}}^2 - R_{\text{in}}^2\right)M^{3/2}} \right) \quad (4)$$

Here, R_p, k_2, and Q refer to Saturn's radius, degree-2 tidal potential Love number, and bulk tidal quality factor (for solid tides, inverse of the mean angle between the actual and frictionless tidal bulges), respectively. $Q_{i,\text{tide}}$ is the tidal heating rate inside each of the moon's grid zones[62]. The k_2 of Saturn is set to its best estimate of 0.39 (ref.[2]; precision 0.024). The evolution of a moon's orbital eccentricity is governed by:

$$\Delta e = \Delta t \times \left(\frac{-\sum_i Q_{i,\,\text{tide}} a}{GMm\ e} + \frac{57}{8}\frac{k_2}{Q}\frac{\sqrt{GM}R_p^5 m\ e}{a^{6.5}} \right) \quad (5)$$

in the absence of moon-moon interactions.

Moon-moon interactions

We have upgraded our code to simulate the internal evolution of N objects simultaneously. The code reads the input file, sets parameters common to the entire system, such as the mass of Saturn; and then calls N parallel instances of the thermal evolution subroutine (here, N = 5). This subroutine is run for one time step; it returns the updated orbital parameters (a and e) of its corresponding moon to the main program, which feeds orbital parameters for all moons into each thermal evolution subroutine instance at the next time step. Thus, each moon "sees" where all other moons are in real time, so that mutual gravitational effects can be computed. The parallelization of the code results in simulation times for 5 moons that are about double those for a single object. Each simulation spanning 4.5 Gyr, with 50-year time

steps, takes about 300 CPU hours, or 4 days with a dual 2.4 GHz Intel Xeon 8-core processor (Mac Pro).

Accurately computing mutual gravitational effects between moons would require computing the moons' orbital elements many times along an orbit[63]. The moons' current orbits have periods of 1 to 4.5 days; requiring time steps of ≤ 1 hour. With such small time steps, a simulation spanning 4.5 Gyr would take ≥ 10^8 CPU hours, an impractical amount of time (20 years per simulation on a 1000-core supercomputer). Thus, we compute moon-moon interactions using a simplistic but much faster approximation, which neglects any effects other than mean-motion resonances such as trapping and secular effects[7]. We assume that resonances occur only if the mean motions of two moons $n_i = \sqrt{GM/a_i^3}$ (neglecting the moons' masses relative to Saturn's) remain commensurate to within less than 1% over one time step Δt; i.e. $|j\,n_1 - (j+k)\,n_2| < 0.01\,n_1/N_{\text{orbits}}$ if $n_1 > n_2$; or $|(j+k)\,n_1 - j\,n_2| < 0.01\,n_1/N_{\text{orbits}}$ otherwise, with j and k positive integers, and $N_{\text{orbits}} = \Delta t/(2\pi/n_1)$ the number of orbits traveled over one time step. Thus, the right-hand side of each condition is implemented as $(0.01\,2\pi/\Delta t)$. We consider only low-order resonances: $j \leq 5$ and $k \leq 3$, i.e. from 2:1 to 8:5. Furthermore, we assume that these interactions only act to increase eccentricities, as described by equations (4) and (5) of Charnoz et al.[7]:

$$\frac{\Delta e}{\Delta t} = Max\left(0, \frac{\Delta v/v_k - e}{T_{\text{res}}}\right) \quad (6)$$

where T_{res} is the period between two conjunctions between moons, equated to $2\pi/(j\,n_1)$ if $n_1 > n_2$ or $2\pi/(j\,n_2)$ otherwise; v_k is the Keplerian velocity of the moon experiencing the perturbation, approximated as $n \times a$; and Δv is the velocity perpendicular to orbital motion imparted by repeated encounters between two moons[64]:

$$\Delta v = 2\frac{m_2 v_{\text{rel}}}{m_1 + m_2}\sin\chi\sqrt{1-\sin^2\chi} \quad (7)$$

where m_1 is the mass of the moon and m_2 that of the moon it interacts with, $v_{\text{rel}} = |n_1 a_1 - n_2 a_2|$ the relative orbital velocity between the two interacting moons, and

$$\sin\chi = \left(1 + \frac{P^2 v_{\text{rel}}^4}{G^2(m_1+m_2)^2}\right)^{-1/2} \quad (8)$$

with P the impact parameter or distance of closest approach between the moons, approximated as $|a_1 - a_2|$. The above two equations are equations 1 and 2 of Greenberg et al. [64]. Thus, the evolution of a moon's orbital eccentricity is governed by:

$$\Delta e = \Delta t \times \left(\frac{-\sum_i Q_{i,\ \mathrm{tide}} a}{GMm\ e} + \frac{57}{8} \frac{k_2}{Q} \frac{\sqrt{G/M} R_p^5 m\ e}{a^{6.5}} + \mathrm{Max}\left(0, \frac{\Delta v / v_k - e}{T_{\mathrm{res}}}\right) \right) \quad (9)$$

These terms describe tidal dissipation inside the moon (as a function of the tidal heating rate), tidal dissipation inside Saturn, and gravitational interactions with other moons, respectively. For the mid-sized moons, $\Delta v / v_k$ has values of ~ 10^{-6} to a few 10^{-5}, so only moons with $e < 10^{-6} - 10^{-5}$ are affected by interactions with other moons.

A drawback of this model is that the overall scaling of eccentricity increases, a physical quantity, depends on the chosen time step, a numerical construct. To achieve results that are physically realistic at the order-of-magnitude level, we adjusted the time step so that the maximum eccentricities excited by mutual interactions are often at least 10^{-3}, can be higher than 0.1, and rarely exceed 1 (ejection from the system). Such outcomes are suggested by our simulations with a more accurate averaged Hamiltonian dynamical model[28] (Supplementary Section 1) validated against previous computations of the orbital evolution of Saturn's mid-sized moons[28;66] (Supplementary Fig. 6), and by previous studies using N-body simulations of the Saturn[3;67] and Uranus systems[68], and planetary systems in general[69;70]. The resonance period T_{res} being about 10^5 s, the third term in equation (9) is of order 10^{-11} to a few 10^{-10}, so a realistic behavior is reproduced by choosing a time step of Δt = 50 years ≈ 1.6×10^9 s.

Eccentricity increases due to moon-moon interactions are assumed instantaneous, i.e. as reaching maximum eccentricity within one time step due to repeated conjunctions during that time step. This assumption is validated a posteriori by comparison with averaged Hamiltonian model simulations, in which eccentricity increases are also fast. In simulations with either model (compare Fig. 2 to Supp. Fig. 7, 8, and 9, and compare Fig. 3 and Supp. Fig. 3 to Supp. Fig. 10 and 11, respectively), moon-moon interactions (a) are more likely to occur if the moons' eccentricities are low before resonance[71], (b) can increase them to above 0.1, inducing melting in the moons' shells, and (c) tend to perturb orbits more for a moon in closer conjunction with a relatively more massive moon. While no simulation with the averaged Hamiltonian model resulted in sufficient excitation of Enceladus' eccentricity to induce melting in its shell, the few simulations carried out sampled only a tiny fraction of an immense orbital parameter space (e.g. behavior of Saturn's Q and starting moon longitudes of pericenter and mean anomaly), which cannot be explored by a systematic or Monte Carlo approach with our computational capabilities.

In both models, even though computed eccentricities can reach values above 0.5, we truncate tidal equations to their lowest-order terms, assuming $e \ll 1$. At e = 0.5, accounting for eccentricity terms to order 10 yields an energy dissipation about 25 times higher than by truncating the tidal heating term to order 2 (equation 26 of Wisdom[72]). In this case, our truncation is equivalent to underestimating eccentricities by a factor of ~5. This is within the order-of-magnitude uncertainties of the above moon-moon interaction model, and partly compensates any overestimation of eccentricities (the magnitude of the eccentricities effectively accounted for in heating terms does not exceed ~ 0.1).

Our models neglect moons exterior to Rhea's orbit, in particular Titan. Secular interactions with Titan may keep Rhea's eccentricity non-negligible[65]. However, a control simulation with a sixth moon with the size (radius 2576 km) and bulk density (1879 kg m^{-3}) of Titan (Supplementary Fig. 4) produces similar outcomes as our canonical results (Fig. 2). Finally, our models neglect the growth of the moons during accretion. Accretion is assumed completed before a simulation starts, or before a late-forming moon is spawned. This limitation could matter most for late-forming moons such as Mimas. Even then, the effect on the results is small, as quantified by control simulations carried out without Mimas (i.e. moon with zero mass at the onset of accretion; compare Supplementary Figures 1 and 6). This assumption also prevents us from seeking explanations to the puzzling lack of trend between the moons' bulk densities (accreted rock content) and their masses or semi-major axes[7;73;74].

Other assumptions & initial conditions

The moons are assumed to accrete hydrated rock (possibly hydrated in satellitesimals, in which ice may have been melted due to the decay of short-lived radionuclides or accretional heat). Moon cores are assumed to retain 25 vol.% of pore water. This assumption was previously made to assess whether the resulting increased tidal dissipation in Enceladus' core could explain its level of geological activity[37;38]. Interestingly, this model yields differentiated internal structures compatible with observational constraints for all five moons, in particular the low density of Enceladus' core[8–10;13;47] and Rhea's low degree of differentiation[12].

We do not attempt to realistically relate variations in Q to changes in Saturn's interior over time, and neglect any variation of Q with excitation frequency. The dependence on frequency seems small at the present day at the orbital frequencies of Enceladus, Tethys, Dione, and (to a lesser extent) Rhea[2]. Saturn's internal structure and evolution (presence and extent of a core, contraction over time, helium separation from hydrogen) remain too poorly constrained to fully match predictions and observations of Q as a function of frequency and time[2;75]. Thus, future work could more realistically simulate Saturn's Q.

Starting orbital semi-major axes are chosen so that the moons reach their current positions at the present day. A common canonical starting eccentricity $e = 0.016$ is assumed for all moons, chosen so that Mimas reaches its present-day eccentricity of 0.0196 without significant internal tidal dissipation or moon-moon interactions. For late-forming moons, this value is consistent with an eccentricity increase away from Saturn for small moons between the outer edge of the rings and Mimas (Supplementary Fig. 12). For primordial moons forming in Saturn's accretion disk, a similar value of ≈ 0.02 reflects a balance between mutual gravitational interactions and eccentricity damping by density waves in the disk, in the absence of significant early tidal dissipation inside the moons[5].

If a moon forms from the rings, the ring mass is decreased instantaneously by the mass of this moon. Thus, the initial ring mass is chosen to be the final ring mass, constrained to $\geq 4.5 - 8 \times 10^{19}$ kg (ref.[35]), augmented by those of the late-forming moons[5;7;76;77]. We also run simulations with final ring masses as low as 1×10^{19} kg to approximate the surface density of the A ring, which is several times lower than that of the B ring but governs moon-ring

interactions for $a > 190000$ km. Moons spawned from rings are assumed to form differentiated (layered) following the rock seed accretion scenario[7], although moons may get their rock content from subsequent exogenic input[74]. Starting semi-major axes are typically around 160000 km, which is slightly higher than the dense rings' current outer radius (135000–140000 km) to account for the fact that the moon may still be accreting material after leaving the rings; we assume it is fully formed by the time its semi-major axis reaches 160000 km. Primordial moons are assumed to form homogeneous. In either case, the moons are assumed to accrete with 20% porosity, which is allowed to compact over time at rates that depend on material viscosity[20].

For simplicity, surface temperatures are assumed constant over time, even though there were likely variations in mean surface albedo, heliocentric distance of the Saturn system, and solar luminosity. We set them to the effective temperatures determined from measured albedos[78], but equate Enceladus' surface temperature to Tethys' (the next brightest of the five moons) on the grounds that reflective snow at Enceladus' surface may be due to recent cryovolcanic activity.

Data and code availability

All data generated or analysed during this study are included in this published article and supplementary files. The code used to generate those data is freely available at https://github.com/MarcNeveu/IcyDwarf.

Supplementary Material

Refer to Web version on PubMed Central for supplementary material.

Acknowledgements

This research was funded by A.R.R.'s startup funds at Arizona State University and NASA's Cassini Data Analysis Program program award NNX16AI42G. We thank four anonymous reviewers and Associate Editor L. Maltagliati for comments that substantially improved this article, and S. Desch for providing access to the computers on which the model was developed and simulations were run.

References

[1]. Kirchoff MR, Bierhaus EB, Dones L, Robbins SJ, Singer KN, Wagner RJ, & Zahnle KJ Cratering Histories in the Saturnian System In Enceladus and the Icy Moons of Saturn, pages 267–284. U. of Arizona Press (2018).

[2]. Lainey V, Jacobson RA, Tajeddine R, Cooper NJ, Murray C, Robert V, Tobie G, Guillot T, Mathis S, Remus F, Desmars J, Arlot J-E, De Cuyper J, Dehant V, Pascu D, Thuillot W, Le Poncin-Lafitte C, & Zahn J-P New constraints on Saturn's interior from Cassini astrometric data. Icarus, 281, 286–296 (2017). http://dx.doi.Org/10.1016/j.icarus.2016.07.014.

[3]. Ćuk M, Dones L, & Nesvornỳ D Dynamical evidence for a late formation of Saturn's moons. Astrophys. J, 820, 97 (2016). 10.3847/0004-637X/820/2/97.

[4]. Asphaug E & Reufer A Late origin of the Saturn system. Icarus, 223, 544–565 (2013). http://dx.doi.org/10.1016Zj.icarus.2012.12.009.

[5]. Canup RM Origin of Saturn's rings and inner moons by mass removal from a lost Titan-sized satellite. Nature, 468, 943–946 (2010). 10.1038/nature09661. [PubMed: 21151108]

[6]. Movshovitz N, Nimmo F, Korycansky DG, Asphaug E, & Owen JM Disruption and reaccretion of midsized moons during an outer solar system Late Heavy Bombardment. Geophys. Res. Lett, 42, 256–263 (2015). 10.1002/2014GL062133.

[7]. Charnoz S, Crida A, Castillo-Rogez JC, Lainey V, Dones L, Karatekin Ö, Tobie G, Mathis S, Le Poncin-Lafitte C, & Salmon J Accretion of Saturn's mid-sized moons during the viscous spreading of young massive rings: Solving the paradox of silicate-poor rings versus silicate-rich moons. Icarus, 216, 535–550 (2011). 10.1016/j.icarus.2011.09.017.

[8]. Beuthe M, Rivoldini A, & Trinh A Enceladus's and Dione's floating ice shells supported by minimum stress isostasy. Geophys. Res. Lett, 43, 10088–10096 (2016). 10.1002/2016GL070650.

[9]. Čadek O, Tobie G, Van Hoolst T, Massé M, Choblet G, Lefèvre A, Mitri G, Baland R-M, Běhounková M, Bourgeois O, & Trinh A Enceladus's internal ocean and ice shell constrained from Cassini gravity, shape, and libration data. Geophys. Res. Lett, 43, 5653–5660 (2016). 10.1002/2016GL068634.

[10]. McKinnon WB Effect of Enceladus's rapid synchronous spin on interpretation of Cassini gravity. Geophys. Res. Lett, 42, 2137–2143 (2015). 10.1002/2015GL063384.

[11]. Tajeddine R, Rambaux N, Lainey V, Charnoz S, Richard A, Rivoldini A, & Noyelles B Constraints on Mimas' interior from Cassini ISS libration measurements. Science, 346, 322–324 (2014). 10.1126/science.1255299. [PubMed: 25324382]

[12]. Tortora P, Zannoni M, Hemingway D, Nimmo F, Jacobson RA, Iess L, & Parisi M Rhea gravity field and interior modeling from Cassini data analysis. Icarus, 264, 264–273 (2016). 10.1016/j.icarus.2015.09.022.

[13]. Thomas PC, Tajeddine R, Tiscareno MS, Burns JA, Joseph J, Loredo TJ, Helfenstein P, & Porco C Enceladus's measured physical libration requires a global subsurface ocean. Icarus, 264, 37–47 (2016). 10.1016/j.icarus.2015.08.037.

[14]. Hsu H-W, Postberg F, Sekine Y, Shibuya T, Kempf S, Horányi M, Juhász A, Altobelli N, Suzuki K, Masaki Y, Kuwatani T, Tachibana S, Sirono S, Moragas-Klostermeyer G, & Srama R Ongoing hydrothermal activities within Enceladus. Nature, 519, 207–210 (2015). 10.1038/nature14262. [PubMed: 25762281]

[15]. Waite JH, Glein CR, Perryman RS, Teolis BD, Magee BA, Miller G, Grimes J, Perry ME, Miller KE, Bouquet A, Lunine JI, Brockwell T, & Bolton SJ Cassini finds molecular hydrogen in the Enceladus plume: Evidence for hydrothermal processes. Science, 356, 155–159 (2017). 10.1126/science.aai8703. [PubMed: 28408597]

[16]. Porco CC, Helfenstein P, Thomas PC, Ingersoll AP, Wisdom J, West R, Neukum G, Denk T, Wagner R, Roatsch T, Kieffer S, Turtle E, McEwen A, Johnson TV, Rathbun J, Veverka J, Wilson D, Perry J, Spitale J, Brahic A, Burns JA, DelGenio AD, Dones L, Murray CD, & Squyres S Cassini observes the active south pole of Enceladus. Science, 311, 1393–1401 (2006). 10.1126/science.1123013. [PubMed: 16527964]

[17]. Bland MT, McKinnon WB, & Schenk PM Constraining the heat flux between Enceladus' tiger stripes: Numerical modeling of funiscular plains formation. Icarus, 260, 232–245 (2015). 10.1016/j.icarus.2015.07.016.

[18]. Howett CJA, Spencer JR, Pearl J, & Segura M High heat flow from Enceladus' south polar region measured using 10–600 cm^{-1} Cassini/CIRS data. J. Geophys. Res.-Planet, 116, E03003 (2011). 10.1029/2010JE003718.

[19]. Spencer JR, Howett C, Verbiscer A, Hurford TA, Segura M, & Spencer DC Enceladus heat flow from high spatial resolution thermal emission observations. In EPSC Abstracts, 8, 840–1 (2013).

[20]. Neveu M & Rhoden AR The origin and evolution of a differentiated Mimas. Icarus, 296, 183–196 (2017). 10.1016/j.icarus.2017.06.011.

[21]. Rhoden AR, Henning W, Hurford TA, Patthoff DA, & Tajeddine R The implications of tides on the Mimas ocean hypothesis. J. Geophys. Res.-Planet, 122, 400–410 (2017). 10.1002/2016JE005097.

[22]. Czechowski L & Witek P Comparison of early evolutions of Mimas and Enceladus. Acta Geophys, 63, 900–921 (2015). 10.1515/acgeo-2015-0024.

[23]. Malamud U & Prialnik D Modeling serpentinization: Applied to the early evolution of Enceladus and Mimas. Icarus, 225, 763–774 (2013). 10.1016/j.icarus.2013.04.024.

[24]. Schubert G, Anderson JD, Travis BJ, & Palguta J Enceladus: Present internal structure and differentiation by early and long-term radiogenic heating. Icarus, 188, 345–355 (2007). 10.1016/j.icarus.2006.12.012.

[25]. Shoji D, Hussmann H, Sohl F, & Kurita K Non-steady state tidal heating of Enceladus. Icarus, 235, 75–85 (2014). 10.1016/j.icarus.2014.03.006.

[26]. Travis BJ & Schubert G Keeping Enceladus warm. Icarus, 250, 32–42 (2015). 10.1016/j.icarus.2014.11.017.

[27]. Zhang K & Nimmo F Late-stage impacts and the orbital and thermal evolution of Tethys. Icarus, 218, 348–355 (2012). 10.1016/j.icarus.2011.12.013.

[28]. Meyer J & Wisdom J Tidal evolution of Mimas, Enceladus, and Dione. Icarus, 193, 213–223 (2008). 10.1016/j.icarus.2007.09.008.

[29]. Zhang Z, Hayes AG, Janssen MA, Nicholson PD, Cuzzi JN, de Pater I, Dunn DE, Estrada PR, & Hedman MM Cassini microwave observations provide clues to the origin of Saturn's C ring. Icarus, 281, 297–321 (2017). 10.1016/j.icarus.2016.07.020.

[30]. Zhang Z, Hayes AG, de Pater I, Dunn DE, Janssen MA, Nicholson PD, Cuzzi JN, Butler BJ, Sault RJ, & Chatterjee S VLA multi-wavelength microwave observations of Saturn's C and B rings. Icarus, 317, 518–548 (2019). 10.1016/j.icarus.2018.08.014.

[31]. Charnoz S, Morbidelli A, Dones L, & Salmon J Did Saturn's rings form during the Late Heavy Bombardment? Icarus, 199, 413–428 (2009). 10.1016/j.icarus.2008.10.019.

[32]. Hyodo R, Charnoz S, Ohtsuki K, & Genda H Ring formation around giant planets by tidal disruption of a single passing large Kuiper belt object. Icarus, 282, 195–213 (2017). 10.1016/j.icarus.2016.09.012

[33]. Dubinski J A recent origin for Saturn's rings from the collisional disruption of an icy moon. Icarus, 321, 291–306 (2019). 10.1016/j.icarus.2018.11.034.

[34]. Fuller J, Luan J, & Quataert E Resonance locking as the source of rapid tidal migration in the Jupiter and Saturn moon systems. Mon. Not. R. Astron. Soc, 458, 3867–3879 (2016). 10.1093/mnras/stw609.

[35]. Robbins SJ, Stewart GR, Lewis MC, Colwell JE, & Sremčević M Estimating the masses of Saturn's A and B rings from high-optical depth N-body simulations and stellar occultations. Icarus, 206, 431–445 (2010). 10.1016/j.icarus.2009.09.012.

[36]. Grossmann L Saturn's rings are surprisingly young and may be from shredded moons. ScienceNews, 193, 7 (2018). https://www.sciencenews.org/article/saturn-rings-age-young-moons.

[37]. Choblet G, Tobie G, Sotin C, Běhounková M, Čadek O, Postberg F, & Souček O Powering prolonged hydrothermal activity inside Enceladus. Nat. Astron, 1, 841–847 (2017). 10.1038/s41550-017-0289-8.

[38]. Roberts JH The fluffy core of Enceladus. Icarus, 258, 54–66 (2015). 10.1016/j.icarus.2015.05.033.

[39]. Tyler R Comparative estimates of the heat generated by ocean tides on icy satellites in the outer Solar System. Icarus, 243, 358–385 (2014). 10.1016/j.icarus.2014.08.037.

[40]. Sekine Y, Shibuya T, Postberg F, Hsu H-W, Suzuki K, Masaki Y, Kuwatani T, Mori M, Hong PK, Yoshizaki M, Tachibana S, & Sirono S.-i. High-temperature water-rock interactions and hydrothermal environments in the chondrite-like core of Enceladus. Nat. Commun, 6, 8604 (2015). 10.1038/ncomms9604. [PubMed: 26506464]

[41]. Meyer J & Wisdom J Tidal heating in Enceladus. Icarus, 188, 535–539 (2007). 10.1016/j.icarus.2007.03.001.

[42]. Roberts JH & Nimmo F Tidal heating and the long-term stability of a subsurface ocean on Enceladus. Icarus, 194, 675–689 (2008). 10.1016/j.icarus.2007.11.010.

[43]. Dermott SF & Thomas PC The shape and internal structure of Mimas. Icarus, 73, 25–65 (1988). 10.1016/0019-1035(88)90084-X.

[44]. Malhotra R Orbital resonances and chaos in the solar system In Solar System Formation and Evolution: ASP Conference Series (Eds. Lazzaro D, Vieira Martins R, Ferraz-Mello S, & Fernandez J) 149, 37 (1998).

[45]. Thomas PC Sizes, shapes, and derived properties of the saturnian satellites after the Cassini nominal mission. Icarus, 208, 395–401 (2010). 10.1016/j.icarus.2010.01.025.

[46]. Jacobson RA, Antreasian PG, Bordi JJ, Criddle KE, Ionasescu R, Jones JB, Mackenzie RA, Meek MC, Parcher D, Pelletier FJ, Owen WM, Roth DC, Roundhill IM, & Stauch JR The gravity field of the saturnian system from satellite observations and spacecraft tracking data. Astron. J, 132, 2520 (2006). 10.1086/508812.

[47]. Iess L, Stevenson DJ, Parisi M, Hemingway D, Jacobson RA, Lunine JI, Nimmo F, Armstrong JW, Asmar SW, Ducci M, & Tortora P The gravity field and interior structure of Enceladus. Science, 344, 78–80 (2014). 10.1126/science.1250551. [PubMed: 24700854]

[48]. Bland MT, Singer KN, McKinnon WB, & Schenk PM Enceladus' extreme heat flux as revealed by its relaxed craters. Geophys. Res. Lett, 39 (2012). 10.1029/2012GL052736.

[49]. Bland MT, Beyer RA, & Showman AP Unstable extension of Enceladus' lithosphere. Icarus, 192, 92–105 (2007). 10.1016/j.icarus.2007.06.011.

[50]. Giese B, Wagner R, Hussmann H, Neukum G, Perry J, Helfenstein P, & Thomas PC Enceladus: An estimate of heat flux and lithospheric thick-ness from flexurally supported topography. Geophys. Res. Lett, 35, L24204 (2008). 10.1029/2008GL036149.

[51]. White OL, Schenk PM, Bellagamba AW, Grimm AM, Dombard AJ, & Bray VJ Impact crater relaxation on Dione and Tethys and relation to past heat flow. Icarus, 288, 37–52 (2017). 10.1016/j.icarus.2017.01.025.

[52]. Hammond NP, Phillips CB, Nimmo F, & Kattenhorn SA Flexure on Dione: Investigating subsurface structure and thermal history. Icarus, 223, 418–422 (2013). 10.1016/j.icarus.2012.12.021.

[53]. Nimmo F, Bills BG, Thomas PC, & Asmar SW Geophysical implications of the long-wavelength topography of Rhea. J. Geophys. Res.-Planet, 115, E10008 (2010). 10.1029/2010JE003604.

[54]. Desch SJ, Cook JC, Doggett TC, & Porter SB Thermal evolution of Kuiper belt objects, with implications for cryovolcanism. Icarus, 202, 694–714 (2009). https://doi.Org/10.1016/j.icarus.2009.03.009.

[55]. Rubin ME, Desch SJ, & Neveu M The effect of Rayleigh–Taylor instabilities on the thickness of undifferentiated crust on Kuiper Belt Objects. Icarus, 236, 122–135(2014). https://doi.org/10.1016Zj.icarus.2014.03.047.

[56]. Neveu M, Desch SJ, & Castillo-Rogez JC Core cracking and hydrothermal circulation can profoundly affect Ceres' geophysical evolution. J. Geophys. Res.-Planet, 120, 123–154 (2015). URL 10.1002/2014JE004714.

[57]. Lodders K Solar system abundances and condensation temperatures of the elements. Astrophys. J, 591, 1220 (2003). 10.1086/375492.

[58]. Tobie G, Mocquet A, & Sotin C Tidal dissipation within large icy satellites: Applications to Europa and Titan. Icarus, 177, 534–549 (2005). 10.1016/j.icarus.2005.04.006.

[59]. Sabadini R & Vermeersen B Normal mode theory in viscoelasticity In Global Dynamics of the Earth, pages 1–44. Springer (2004).

[60]. Meyer-Vernet N & Sicardy B On the physics of resonant disk-satellite interaction. Icarus, 69,157–175 (1987). 10.1016/0019-1035(87)90011-X.

[61]. Nakajima A, Ida S, Kimura J, & Brasser R Orbital evolution of Saturns mid-sized moons and the tidal heating of Enceladus. Icarus, 317, 570–582 (2019). 10.1016/j.icarus.2018.08.030.

[62]. Henning WG & Hurford T Tidal heating in multilayered terrestrial exoplanets. Astrophys. J, 789, 30 (2014). 10.1088/0004-637X/789/1/30.

[63]. Chambers JE A hybrid symplectic integrator that permits close encounters between massive bodies. Mon. Not. R. Astron. Soc, 304, 793–799 (1999). 10.1046/j.1365-8711.1999.02379.x.

[64]. Greenberg R, Wacker JF, Hartmann WK, & Chapman CR Planetesimals to planets: Numerical simulation of collisional evolution. Icarus, 35, 1–26 (1978). 10.1016/0019-1035(78)90057-X.

[65]. Greenberg R Orbit-orbit resonances in the solar system: Varieties and similarities. Vistas Astron, 21, 209–239 (1977). 10.1016/0083-6656(77)90031-9.

[66]. Zhang K & Nimmo F Recent orbital evolution and the internal structures of Enceladus and Dione. Icarus, 204, 597–609 (2009). 10.1016/j.icarus.2009.07.007.

[67]. Noyelles B, Baillie K, Lainey V, & Charnoz S How Mimas cleared the Cassini Division. In AAS/DPS Meeting Abstracts, 48, 121.07 (2016).

[68]. Dermott SF, Malhotra R, & Murray CD Dynamics of the Uranian and Saturnian satellite systems: A chaotic route to melting Miranda? Icarus, 76, 295–334 (1988). 10.1016/0019-1035(88)90074-7.

[69]. Tsiganis K, Gomes R, Morbidelli A, & Levison HF Origin of the orbital architecture of the giant planets of the Solar System. Nature, 435, 459 (2005). 10.1038/nature03539. [PubMed: 15917800]

[70]. Barnes R, Deitrick R, Greenberg R, Quinn TR, & Raymond SN Long-lived chaotic orbital evolution of exoplanets in mean motion resonances with mutual inclinations. Astrophys. J, 801, 101 (2015). 10.1088/0004-637X/801/2/101.

[71]. Borderies N & Goldreich P A simple derivation of capture probabilities for the j+ 1:j and j+2:j orbit-orbit resonance problems. Celestial Mech, 32, 127–136 (1984). 10.1007/BF01231120.

[72]. Wisdom J Tidal dissipation at arbitrary eccentricity and obliquity. Icarus, 193, 637–640 (2008). 10.1016/j.icarus.2007.09.002.

[73]. Sekine Y & Genda H Giant impacts in the Saturnian system: A possible origin of diversity in the inner mid-sized satellites. Planet. Space Sci, 63, 133–138 (2012). 10.1016/j.pss.2011.05.015.

[74]. Salmon J & Canup RM Accretion of Saturn's inner mid-sized moons from a massive primordial ice ring. Astrophys. J, 836, 109 (2017). 10.3847/1538-4357/836/1/109. [PubMed: 31019332]

[75]. Shoji D & Hussmann H Frequency-dependent tidal dissipation in a viscoelastic Saturnian core and expansion of Mimas' semi-major axis. Astron. Astrophys, 599, L10 (2017). 10.1051/0004-6361/201630230.

[76]. Charnoz S, Salmon J, & Crida A The recent formation of Saturn's moon-lets from viscous spreading of the main rings. Nature, 465, 752–754 (2010). 10.1038/nature09096. [PubMed: 20535205]

[77]. Salmon J, Charnoz S, Crida A, & Brahic A Long-term and large-scale viscous evolution of dense planetary rings. Icarus, 209, 771–785 (2010). 10.1016/j.icarus.2010.05.030.

[78]. Howett CJA, Spencer JR, Pearl J, & Segura M Thermal inertia and bolometric Bond albedo values for Mimas, Enceladus, Tethys, Dione, Rhea and Iapetus as derived from Cassini/CIRS measurements. Icarus, 206, 573–593 (2010). 10.1016/j.icarus.2009.07.016.

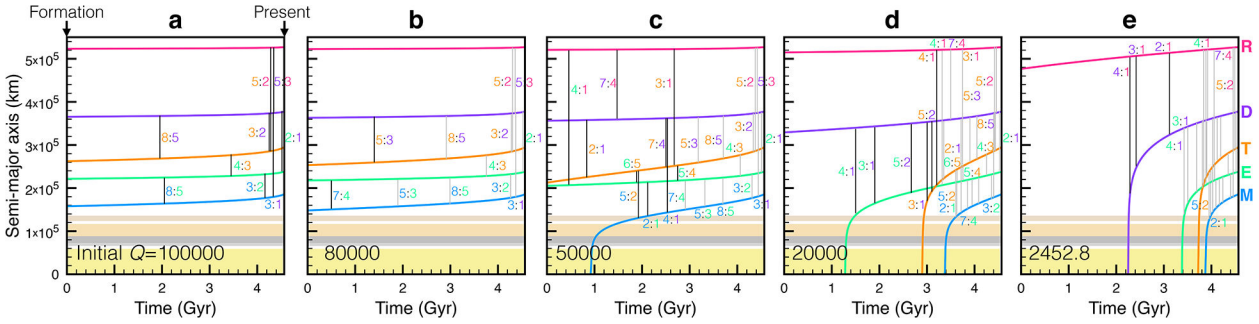

Figure 1. Evolution of the moons' semi-major axes over time due to tidal dissipation inside Saturn.

The color-coding for each moon is indicated by moon initials (R=Rhea, D=Dione, T=Tethys, E=Enceladus, M=Mimas) to the right of panel (e). Tides result in transfer of angular momentum from fast-spinning Saturn into the moons' orbits, increasing semi-major axes at a rate inversely proportional to the tidal Q of Saturn (second term in equation 4). Semi-major axes are shown as a function of time for five initial values of Saturn's Q, all decreasing linearly to 2452.8 at the present day. These simplified models are used to determine appropriate starting moon semi-major axes or formation times for each starting Q. These are not fully accurate because moon-moon and moon-ring interactions are neglected; so is tidal dissipation inside the moons. Accounting for interactions between Enceladus and the present-day ring would result in minimum initial $Q \gtrsim 80000$ (rather than $Q \gtrsim 50000$; panel c) for Enceladus to be primordial. The curves are overlain on color bands depicting Saturn and its rings. Major mean-motion resonances (j: $j + k$ for $j \leq 5$ and $k \leq 3$) are indicated; those already present in panels to the left are grayed out and not all named.

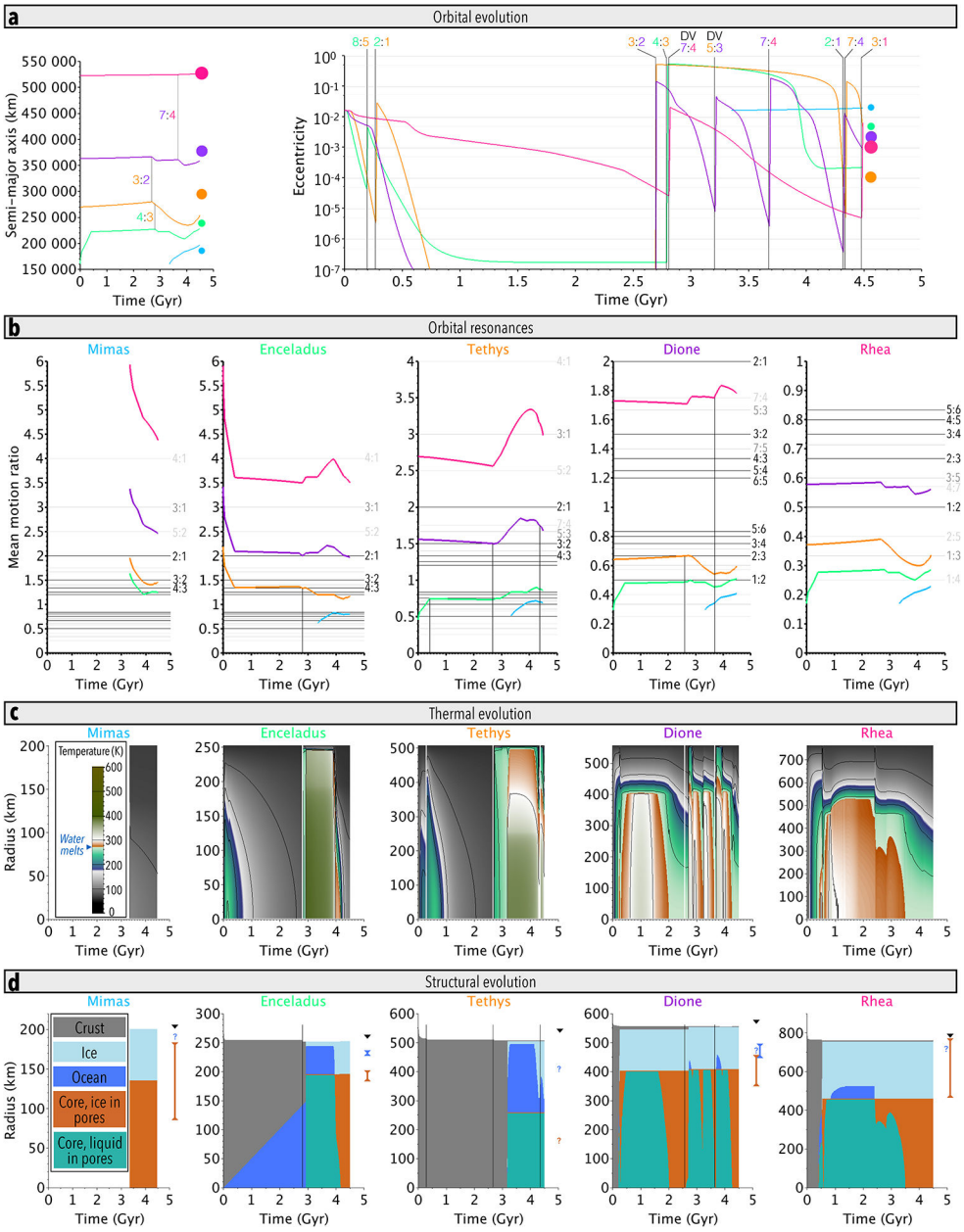

Figure 2. Simulated orbital, structural, and thermal evolution of Saturn's mid-sized moons for an initial Saturn *Q* of 80000 decreasing linearly to today's ~ 2450 provide a close match to observational constraints.

The final ring mass is set to 1×10^{19} kg. In this case all moons but Mimas are primordial (Table 1). (a) Colored lines: orbital semi-major axes and eccentricities over time (blue: Mimas; green: Enceladus; orange: Tethys; purple: Dione; pink: Rhea). Circles: observed present-day positions; the size scales with moon size (Table 1). (b) Ratios of mean motions of the moon named at the top of each plot to the other moons color-coded as above. Decreasing ratios above 1 or increasing ratios below 1 indicate convergent migration during which resonances can occur. Our rough model computes a few spurious instances of eccentricity excitation during divergent migration; these are indicated ("DV") and seldom

affect the moons' evolutions (Supplementary Section 3). (c) Corresponding internal temperatures (scale bar in the Mimas plot; a switch from green to orange indicates that ice melts). (d) Internal structures as a function of time (gray: undifferentiated; sky blue: ice; blue: ocean–or liquid water if the moon is undifferentiated–; brown: core with pore ice; teal: core with pore liquid water). Bars to the right of each plot indicate observational constraints (Table 1) on the outer radii of the core (brown), ocean (blue), and moon (black). In each panel, resonances that significantly affect orbital, thermal, and/or structural evolution are marked by vertical lines.

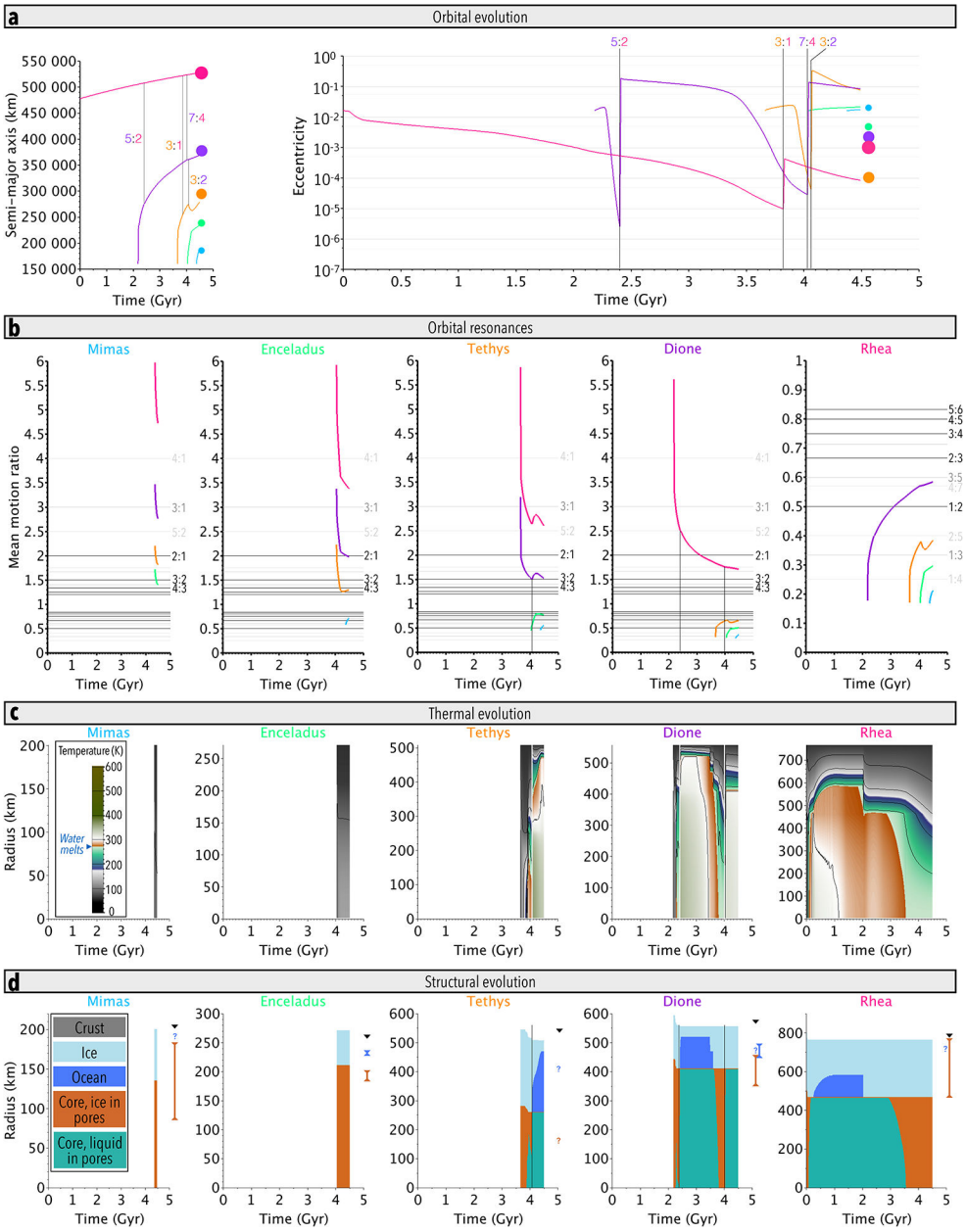

Figure 3. Orbital, structural, and thermal evolution of Saturn's mid-sized moons for an initial Saturn *Q* of 2452.8.

The legend is the same as for Fig. 2. This scenario does not reproduce observed properties of the Saturn system as well. A ring mass of 7×10^{19} kg is assumed, with the sole effect of increasing the rate of migration of late-forming moons, i.e. yielding younger ages for these moons. In this case only Rhea is primordial (Table 1).

Table 1:

Measured interior and orbital characteristics of Saturn's mid-sized moons, and moon-specific physical input parameters.

Observed characteristics are for the present day, except where noted. In the last column are listed the conditions under which simulations are deemed to match measurements.

Parameter	Mimas	Enceladus	Tethys	Dione	Rhea	Condition for match
Observed characteristics						
Mean radius R (km)[a]	198.2	252.0[b]	531.0	561.4	763.5	Within 5%
Mass M (kg)[c]	3.75×10^{19}	1.08×10^{20}	6.17×10^{20}	1.10×10^{21}	2.30×10^{21}	N/A (model input)
Bulk density ρ (kg m^{-3})	1149	1611	985	1478	1237	Within 5%
Core density ρ_c (kg m^{-3})[d]	1200–3300[e]	~2400[f]	Unknown	1940–3120	1240–2100	Within range
Corresponding core radius R_c (km)[h]	82–181	2450[g] 190–192[h] 180–185[i] 183–199[j]	Unknown	344–450[j]	463–758[k]	Within range
Present-day ocean?	Maybe[e]	Yes[f,g,i,j]	Unknown	Maybe[j]	Unknown	Presence or absence
Past near-surface heat flux (mW m^{-2})[l]	Not estimated	≈150[m] 110–400[n]	60[p]	20–60[q] 60[p]	[s]15	Within 20%
Semi-major axis (km)	185539	237948	294660	377400	527040	Within 20%
(Saturn radii)	3.19	4.09	5.06	6.48	9.05	
Eccentricity	0.0196	0.0047	0.0001	0.0022	0.0010	Range overlaps
Assumed quantities						
Porosity-free radius (km)	186.5	252.0	507.7	556.5	762.2	
Initial radius with 20% bulk porosity (km)	200.9	271.5	546.9	599.5	821.1	
Porosity-free bulk density (kg m^{-3})	1378	1611	1127	1517	1267	
Surface temperature[t]	76	68	68	70	72	
Case with initial Q = 80000, initial e = 0.016						
Time of formation (Myr after CAIs)[u]	3450	primordial	primordial	primordial	primordial	
Initial semi-major axis (km)[u]	160000	165000	155000	354000	520000	
Case with constant Q = 2452.8, initial e = 0.016						
Time of formation (Myr after CAIs)[u]	4470	4140	4760	2280	primordial	
Initial semi-major axis (km)[u]	160000	160000	160000	160000	478000	

[a] Thomas[45].

[b] Thomas et al.[13].

[c] Jacobson et al.[46].

[d] Estimated from gravity and libration measurements; the determination of interior models is non-unique. For Dione and Rhea, densities are calculated from reported core radii.

[e] Range of densities explored by Tajeddine et al.[11].

[f] less et al.[47].

[g] McKinnon[10].

[h] Calculated as $R_C = R\,[(\rho - \rho_i)/(\rho_C - \rho_i)]^{1/3}$ assuming an ice shell density $\rho_i = 985$ kg m^{-3}.

[i] Čadek et al.[9].

[j] Beuthe et al.[8].

[k] Tortora et al.[12].

[l] Inferred from analyses of surface topography and crater relaxation.

[m] Bland et al.[48].

[n] Bland et al.[17,49]; Giese et al.[50].

[p] White et al.[51].

[q] Hammond et al.[52].

[s] Nimmo et al.[53].

[t] Effective temperatures, assumed constant over time; Enceladus' surface temperature is equated to that of Tethys (see Methods).

[u] Estimated based on Saturn's Q (Fig. 1) and refined as needed to account for orbital evolution driven by the rings and tidal dissipation inside the moons.

CAIs: Ca-Al-rich inclusions, the oldest known remaining solar system solid material that set the "time zero" of solar system history.

Table 2:

Other model input parameters.

Parameter	Symbol	Value or range	Units	Notes or references
Mass of Saturn	M	5.68×10^{26}	kg	
Radius of Saturn	R_p	58232	km	
Final ring mass	M_{ring}	$10^{19} - 10^{20}$	kg	Robbins et al.[35]
Ring inner edge	R_{in}	92000	km	Inner edge of B ring
Ring outer edge	R_{out}	140000	km	Radius of F ring
Saturn's initial tidal quality factor	Q	2452.8–200000		Lainey et al.[2]
Initial eccentricity	e	0.016		Canup[5]
Initial rock grain density	ρ_r	2900	kg m^{-3}	Hydrated rock
Initial ice grain density	ρ_i	985	kg m^{-3}	
Water volume fraction in the core	X_{ice}	0.25		
Initial bulk porosity	Φ	0.2		
Initial temperature	T_{init}	100	K	

Table 3:

Match between simulation outcomes and observations with the conditions of Table 1 for the results depicted in Fig. 2 (initial Saturn Q = 80000) and Fig. 3 (constant Saturn Q ≈ 2450).

	Initial Saturn Q = 80000		Constant Saturn $Q \approx 2450$	
Moon	**Orbit**	**Interior**	**Orbit**	**Interior**
Mimas	Match	Match	Match	Match
Enceladus	Match at 3–4 Gyr	Match at 3–4 Gyr	*e* too large	Too cold, no ocean
Tethys	Too close in	Match	Match	Match
Dione	Match at 3–4 Gyr	Match at 3–4 Gyr	Match	Past ocean only
Rhea	Match	Match	Match	Match